A Digital Twin Approach for Online Impedance-Based Stability Analysis of Three-Phase AC Systems

Sergio de Lopez Diz, Roberto Martin Lopez, Francisco Javier Rodriguez Sanchez, *Member, IEEE*, and Emilio Jose Bueno Peña, *Senior Member, IEEE*

***Abstract*—In contemporary electrical distribution systems, multiple parallel inverters collaborate to form an advanced power distribution network, which poses stability challenges. Small-signal analysis is a fundamental method for characterizing interactions between system impedances. In three-phase ac systems, stability assessment involves examining the source-to-load impedance ratio in the complex *dq* plane using the Generalized Nyquist criterion (GNC). In this context, the digital twin (DT) concept is arising as the forefront of energy sector digitization, providing real-time data through high-fidelity models mirroring physical systems. This article presents a stability analysis method employing a DT approach to determine the closed-loop impedance of the physical system and estimate the connected system's equivalent impedance. Broadband excitation based on pseudorandom binary sequences (PRBS) is applied with Fourier techniques for frequency response extraction. Impedance ratio assessment is performed on an edge-computing platform, delivering real-time stability information. Experimental results are provided for a dual-hybrid converter, one operating as a grid-forming system and the other in grid-following mode. The outcomes demonstrate the feasibility and potential of the proposal as a foundational approach to enhance robustness based on stability indexes.**

***Index Terms*—Digital twin (DT), edge-computing, real-time, small-signal stability, three-phase electric systems.**

I. Introduction

THE ongoing advancements in semiconductor technologies and inverter design have enabled the growth and diversification of applications within ac-distributed power systems. These applications can be found in several novel and emerging fields, such as renewable energy generation [1], smart grids [2], and the integration of prosumers [3].

Manuscript received 17 January 2024; revised 5 April 2024 and 17 April 2024; accepted 18 April 2024. This work was supported by the Spanish Ministry of Science, Innovation and Universities, under Grant PID2021-125628OB-C22, Grant TED2021-130610B-C21, and Grant PID2022-139575OB-I00 GEMECOP. *(Corresponding author: Sergio de Lopez Diz.)*

The authors are with the University of Alcala, 28801 Alcalá de Henares, Spain (e-mail: s.lopezd@edu.uah.es).

Color versions of one or more figures in this article are available at https://doi.org/10.1109/TIE.2024.3395755.

Digital Object Identifier 10.1109/TIE.2024.3395755

AC-distributed power systems commonly rely on the synchronized operation of multiple paralleled inverters. In certain applications, such as large-scale photovoltaic or wind power plants, the system may encompass a substantial number of inverters, ranging from hundreds to thousands, to amplify the overall power generation capacity. Typically, these inverters are individually designed taking into consideration their independent stability.

Nevertheless, the deployment of parallelized inverters gives rise to dynamic interactions among them, potentially resulting in system performance degradation or even instability, as observed in distribution systems [4]. This phenomenon underscores the significance of addressing the interplay and stability concerns when integrating various converters. Consequently, the analysis of small-signal stability is critical in shaping the design and enhancing the performance of three-phase power conversion systems (PCS). The more practical method is the impedance-based stability analysis, which was initially applied in dc systems [5] and has been adapted for use in ac systems. A key benefit of this methodology lies in its inherent modeling of all circuit elements, encompassing both physical components and control systems. For three-phase ac systems, stability based on impedance can be expressed by using the *dq* frame source and load impedances.

In relation to the above, it is necessary to consider the growing demand for the implementation of real-time analysis approaches that rely on continuous, ongoing measurements and the online estimation impedances. These stability indicators find valuable applications in advanced system monitoring, preemptive fault mitigation, and dynamic control strategies. Incorporating digital techniques, the online identification and analysis can seamlessly integrate into the inverter controllers.

In the literature, there is a noticeable presence of both parametric and nonparametric approaches aimed at estimating grid impedance from measurement data. These methods consider grid impedance to be equivalent to the load impedance as a preliminary step before performing impedance-based stability analyses. To begin with the parametric perspective, in [6] and [7], recursive-parametric methodologies are introduced. One of the drawbacks associated with parametric estimation lies in the necessity to predefine the parameters to be estimated. This limitation proves inadequate in identifying specific resonances

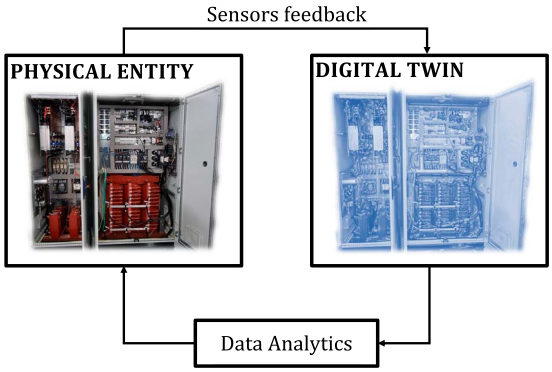

Fig. 1. Example of DT technology applied to a power electronics converter.

that may manifest in highly interconnected converter systems, rendering the method less adaptable to diverse scenarios. In the context of nonparametric approaches, numerous studies have explored the injection of broadband disturbances to obtain the frequency response of a system within a specified frequency range. In [8], an examination of the impact of weak grids on control performance, considering the dynamics introduced by phase-locked loops (PLL) in grid-following (GFL) inverters, is presented. Another illustrative instance is shown in [9], where a comprehensive methodology for characterizing grid impedance in the presence of harmonics and unbalances is described.

For source impedance characterization, numerous studies rely on prior theoretical analyses [10] to establish the converter's impedance. This involves accounting for the dynamics of all loops and linearizing them according to the system's operational state, as evidenced in works such as [11], [12], [13]. Although this method is entirely valid, it may lack flexibility in dynamic systems subject to changing conditions and includes a higher difficulty in terms of consider all the nonlinear effects of the modulation. In this context, the notion of a digital twin (DT) emerges as a new way to analyze stability in real-time.

DT introduces a transformative approach to enhance the performance and reliability of physical energy systems. Initially described as a virtual replica of a physical system that predicts its output characteristics [14], the traditional definition consists of three core elements: the physical system itself, its digital counterpart, and the communication link connecting them. Fig. 1 shows an example of the DT concept applied to a power converter, where the replica can include all conceivable physical and data-driven models emulating the converter behavior.

Over time, this definition has evolved, giving rise to the notion of an intelligent DTs [15]. This updated version of the twin incorporates advanced attributes such as pro-activity, online functionality, goal-driven behavior, and anticipatory capabilities. This abstraction allows a more in-depth understanding of the behavior of energy converters, leading to performance optimization and enhanced reliability through continuous monitoring [16]. In the state of the art, it can be found various proposals for fault diagnosis and condition monitoring applications. Milton et al. [17] introduces a DT model that employs probabilistic simulation with stochastic variables, leveraging a generalized polynomial expansion. The authors have implemented this virtual replica on a field programmable gate array (FPGA), enabling real-time simulations for small power converters. Furthermore, [18] presents a methodology for monitoring the health of components in a buck dc/dc converter. Additionally, [19] introduces a DT of a three-phase converter, with particular attention to the degradation of an LC output filter.

This article introduces a novel application of the DT concept, which has traditionally been focused in the literature on condition monitoring and fault detection. The focus here is on applying the DT approach to system stability analysis, presenting the virtual replica as a tool for deriving robustness metrics in relation to other equipment or the utility grid. The primary robustness metric utilized is the phase margin (PM), acquired through the analysis of the characteristic equation of the system, as detailed in Section II.

The first contribution of this work lies in demonstrating the feasibility of employing the DT approach in stability analysis. Indeed, this enables the rapid and accurate determination of the impedance of the physical system being emulated across all feasible operating points, eliminating the need for linearizing the nonlinear elements of the converter control, as is currently used in the literature. This capability is facilitated by the inputs from sensors feeding the DT and the existence of a virtual control precisely mirroring the control employed in the real system. Taking advantage of its integration on the same control board as its physical counterpart, it becomes straightforward to observe the impact of nonlinear system elements such as dead time [20], conduction losses, and switching losses. These elements are inherently integrated into DT, and while theoretically feasible to account for in prior offline modeling, their accurate representation poses greater challenges to obtain.

The second contribution is a comprehensive exploration of the practical implementation of the virtual replica on an edge-computing platform, enabling real-time stability evaluation. The analysis involves estimating source-to-load impedances with the support of broadband binary perturbation techniques, addressing the limitations of the current impedance knowledge approach when connected to an unknown system. This proposal holds significance in various applications, particularly in tackling issues related to subsynchronous resonances in wind farms resulting from the introduction of series compensation capacitance. This is crucial when certain information about the grid to which the turbine will connect is not known in advance.

Regarding impedances' estimation for the analysis, it is noteworthy that two sources of perturbation are employed to derive them, considering both the source impedance (DT) and the load impedance (the unknown impedance of the system to which connection is made). These disturbances are simultaneously injected into the digital mirror and the real system to efficiently estimate impedances in a single step. Subsequently, the Generalized Nyquist criterion (GNC) is applied to the eigenvalues of the characteristic equation. This approach provides a detailed understanding of the available stability margin in a single stage, enabling proactive measures to prevent disconnection events. Additionally, it is important to note that the DT allows for the validation of potential changes to the controller before

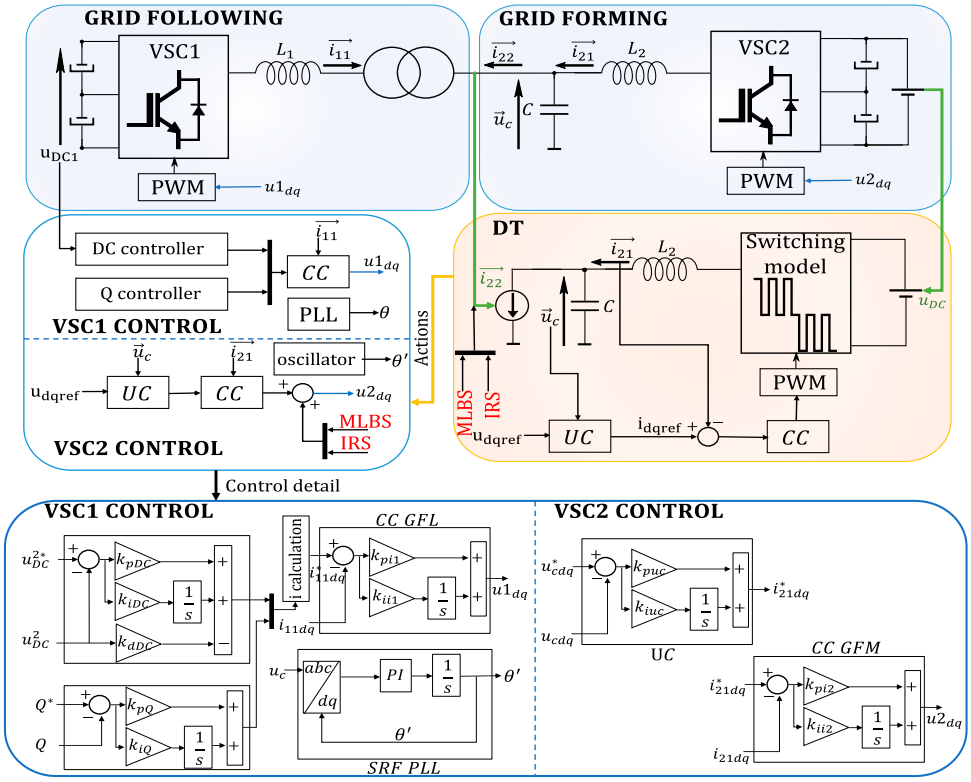

Fig. 2. Experimental system setup for the real-time stability analysis based on DT.

implementing them in the actual plant. This ensures that changes are made in a controlled and safe manner.

The remainder of this article is organized as follows. Section II provides an overview of the system where the DT concept is utilized as a tool for conducting stability assessment. It also offers a brief description of the concepts that will be employed in the analysis. Section III reviews the implementation and the performance of the virtual replica in an edge computing SoC-based platform. Section IV details the frequency-response identification based on orthogonal wideband techniques. Section V presents experimental results on a complete dual hybrid converter with different controller tunings to analyze the stability with the help of the real-time DT. Finally, Section VI draws the fundamental conclusion.

II. System Description and Stability Concepts

Fig. 2 shows the experimental setup aimed at validating the efficacy of the DT in conducting stability analysis for power converters. In this context, two three-level converters, denoted as VSC1 and VSC2 in the figure, are used. VSC1 works as a GFL converter with internal current control and two upper loops, one for dc bus voltage and the other for reactive injection. Notably, a PLL is employed to derive a phase for operation in the complex dq domain. In contrast, VSC2 operates as a grid forming (GFM), regulating the converter output voltage through internal current control and an upper voltage loop. Additionally, it is included the detail of the control loops implemented in each VSC, where it should be noted that the control structure of CC GFL, UC, and CC GFM is represented using complex control constants, nonetheless, in the real system implementation it is divided into the d-axis and q-axis including the cross-coupling term between them. It is important to note that this setup is just one of many possible connections to validate the system for robustness verification using a DT approach.

The DT is employed as a precise emulation of its physical counterpart, specifically the GFM converter. Sensor inputs, highlighted by green lines in the scheme, encompass crucial parameters such as the voltage measured on the dc bus and the output currents from the LC filter. It is imperative to underscore the presence of a virtual control system within the digital replica, mirroring the exact control configuration of the physical converter. This seamless integration is made possible through the implementation in an edge-computing platform, positioning the twin replica as a tool for obtaining a robustness metric of the system.

The establishment of a bidirectional connection between the real and virtual domains is achieved through the modification of the real system's behavior, as depicted by the yellow line in the diagram. This process results in a comprehensive DT model, constituting a thorough and synchronized representation of the physical system within the virtual realm.

Finally, the source/load impedances for the comprehensive stability analysis are derived through the injection of orthogonal sequences. Specifically, the first sequence, referred to as maximum length binary sequence (MLBS) [21], is introduced into the D channel of the system magnitudes, while the second sequence, inverse-repeat sequence (IRS), is injected into

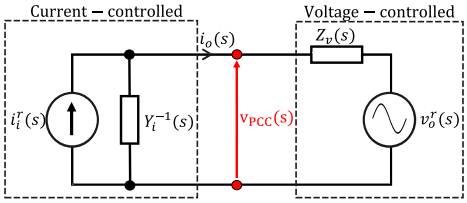

Fig. 3. Interconnection of current-controlled and voltage-controlled systems.

the Q channel. The fundamental rationale for simultaneously introducing two different PRBS-type perturbations into the D and Q channels is to minimize the measurement time compared to sequentially applying a single signal to both channels [22]. This approach takes advantage of the design of orthogonal signals (MLBS and IRS) that do not interfere with each other, thereby optimizing efficiency. In addition, given the potential for impedance change during the insertion of noise, simultaneous insertion in both the D and Q components ensures a uniform effect across all impedance components. This consideration is particularly valuable when treating the impedance as a 2 x 2 matrix in the DQ domain.

In the context of obtaining the impedance for the GFL system, perturbations are directly applied to the u_{2dq} modulating signals. Conversely, for the attainment of the equivalent GFM impedance, perturbations are introduced into the input current signals of the DT. Section IV provides a more in-depth exploration of the physical voltage and current quantities used, along with a detailed description of the design aspects of the perturbations.

With regard to the fundamental stability concepts, this article employs the theoretical basis of impedance-based analysis, introduced in [23] by establishing the interaction between voltage-controlled and current-controlled systems, as illustrated in Fig. 3.

These systems are modeled using Thevenin and Norton equivalent circuits, respectively. The stability condition for the interconnected system is derived from the voltage dynamics at the point of common coupling (PCC) in Laplace domain, expressed as a function of the complex variable s

$$v_{\mathrm{PCC}}(s) = \frac{Z_v(s)}{1 + Z_v(s)Y_i(s)} i_i^r(s) + \frac{1}{1 + Z_v(s)Y_i(s)} v_o^r(s) \quad (1)$$

where v_o^r is the output voltage reference and i_i^r is the current reference of the current-controlled system. Hence, the interconnected subsystems will be stable if the characteristic polynomial $1 + Z_v(s)Y_i(s) = 0$ is Hurwitz, in other words, the eigenvalues must comply with the GNC [24]. It is important to note that stability analysis can also be conducted by modeling the interconnection of the two systems as Thevenin equivalents, with controlled voltage sources. Please note that the characteristic polynomial will be different from that shown in (1). However, once the source/load impedances are identified, the modeling of this interconnection can always be adapted so that the proposed method can be applied in a general manner.

As we are dealing with a multiple-input-multiple-output (MIMO) problem, we can calculate the eigenvalues that will

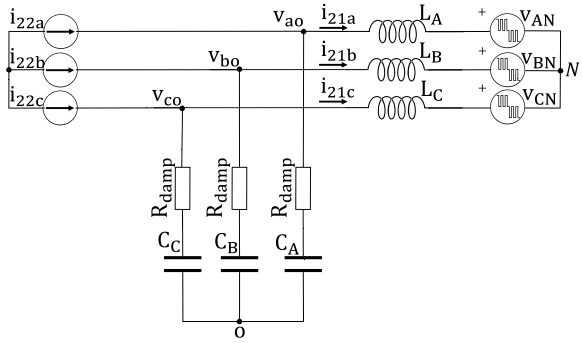

Fig. 4. Equivalent circuit of the GFM converter.

enable to verify the system's stability online as follows:

$$\lambda_1, \lambda_2 = \frac{a+d}{2} \pm \frac{\sqrt{(a-d)^2 + 4bc}}{2} \quad (2)$$

where the variables a, b, c, and d are defined as follows:

$$\begin{bmatrix} a & b \\ c & d \end{bmatrix} = \begin{bmatrix} Z_{v-dd}(s) & Z_{v-dq}(s) \\ Z_{v-qd}(s) & Z_{v-qq}(s) \end{bmatrix} \begin{bmatrix} Y_{i-dd}(s) & Y_{i-dq}(s) \\ Y_{i-qd}(s) & Y_{i-qq}(s) \end{bmatrix}. \quad (3)$$

After obtaining the eigenvalues, we check for the most critical point of instability, which is the one closest to enveloping the point $(-1,0j)$ in the Nyquist diagram.

III. DT Modeling and Performance

The development of the closed-loop DT requires simplifications to accommodate the real-time execution constraints of an edge-computing platform. The fundamental complexity reduction involves expressing the VSC output voltages (v_{AN}, v_{BN}, and v_{CN}) by means of switching functions. The use of this technique establishes a simple and flexible way to represent converter switching, particularly in complex multilevel topologies where real-time execution poses significant challenges [25]. Fig. 4 shows the equivalent circuit of the GFM converter.

The DT modeling framework can be divided into three distinct parts.

1) Plant modeling; 2) the PWM stage; and 3) the virtual control loop.

First, the plant dynamics are modeled with a state-space representation as follows:

$$\begin{aligned} \frac{dx(t)}{dt} &= A_{\sigma(t)}x(t) + B_{\sigma(t)}u(t) \\ y(t) &= Cx(t) + Du(t) \end{aligned} \quad (4)$$

where $x(t)$ describes the continuous states of the circuit, $u(t)$, the inputs of the model, $y(t)$, the outputs of the plant and $\sigma(t)$ indicates the ability to dynamically adjust the matrices based on real-time variations in the passive elements of the plant. Further details on the plant modeling can be found in [19].

Second, the PWM stage involves expressing the output voltages of the converter as a function of the switching of the power devices. Given that this article focuses on three-level ac/dc converters utilizing SPWM modulation (defining a modulating

waveform v_{mod}), the switching pulses can be defined by means of switching functions as follows:

$$S_x = \begin{cases} 1, & T_{x1}, T_{x2} = \text{ON} \\ 0, & T_{x2}, T_{x3} = \text{ON} \\ -1, & T_{x3}, T_{x4} = \text{ON} \end{cases} \tag{5}$$

where "0" and "1" states indicate the OFF and ON conditions, respectively, and T_1, T_2, T_3, T_4 represent the switching devices for each leg. In the pursuit of building a high-fidelity DT, integration of the dead-time effect into the digital domain is imperative. This effect is included following the details in [19].

Later on, the output voltages v_{AN}, v_{BN}, and v_{CN} can be obtained as follows:

$$v_{\text{XN}} = \begin{cases} udc_P, & S_x = 1 \\ udc_N, & S_x = -1 \\ 0, & S_x = 0 \end{cases} \tag{6}$$

where x represents the three phases a, b, and c and udc_P and udc_N are directly the voltage measurements of the dc semibuses.

Third, the virtual control, responsible for generating the modulating signals used in the PWM stage, precisely mirrors the control system operating on the real system. Its purpose is to faithfully emulate the behavior of the GFM converter. The control architecture adheres to a straightforward cascade structure, incorporating an inner current loop and an upper voltage control to shape the grid, as illustrated in Fig. 2.

The DT is seamlessly integrated into a Zynq-based edge-computing development board known as Microzed. This platform features a dual-ARM core, with the processing system (PS) on one side and programmable logic (PL) on the other, comprising two I/O banks and various interfaces.

The PL side includes intellectual properties (IPs) facilitating PWM generation, signal acquisition control, and interrupt management for executing the DT in the PS domain. Simultaneously, the PS side is employed for IPs configuration, operating system integration (Linux), DT implementation and the execution of bare-metal code responsible for implementing the control algorithms for both the physical converter and the virtual replica itself. Fig. 5 presents a simplified illustration of the architecture employed for incorporating a DT within a cost-effective edge-computing framework. The infrastructure follows an asymmetric multiprocessing (AMP) design. On the one hand, one of the cores, denoted as CPU0, acts as a master and runs an operating system, namely Linux to implement the stability analysis layer of the system. On the other hand, the other core acting as slave (named CPU1) integrates the DT and the control algorithms of the physical converter. For this application, the time step of the DT is established at 2.5 μs considering both the limitations of the available hardware and the requirement to perform a stability analysis. Certainly, the minimum execution time of the DT relies entirely on both the platform and the model's complexity, alongside any nonlinear elements incorporated in the virtual representation. When dealing with a more intricate converter representation or topology, a larger time step may be required if utilizing the same edge-computing board.

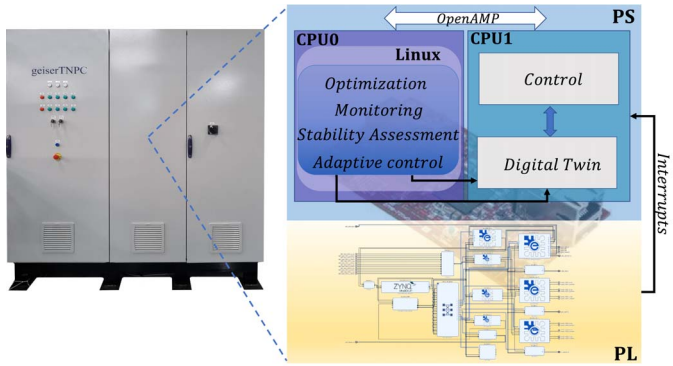

Fig. 5. Implementation of the DT on an edge-computing platform.

Subsequently, to ensure a precise assessment, it is imperative to verify the similarity between the virtual representation and the physical system. Consequently, Fig. 6 illustrates an initial comparison between the output waveforms of the DT and those observed from the real VSC.

The similarity between the digital copy and the physical counterpart is evidenced by the close alignment of signals, affirming the accurate definition and implementation of the modeling task. This allow reliance on the accuracy of the impedance obtained through the DT for use in online stability analysis and it underscores the effectiveness of the tool for solving stability issues.

IV. Frequency Response Identification

The use of the dq-frame representation provides a convenient way for straightforward small-signal analysis. In this context, introducing small perturbations becomes ideal for deriving the source/load impedances of the system.

A. PRBS-Based Classical Method

Following the classical PRBS approach, the system is perturbed by injections of d- and q-components, denoted as $xd(n)$ and $xq(n)$. These injections result in corresponding output responses, namely $yd(n)$ and $yq(n)$. These signals are buffered and subsequently transformed to the frequency domain by applying the Discrete Fourier Transformation (DFT). In the literature, most works introduce these disturbances mainly in the current references of the innermost current loop of the converter to monitor the system's response [26]. However, it is important to note that disturbances can be applied to any control pathway.

Concerning the perturbation type, MLBS frequently represents the optimal choice to maximize signal power while adhering to time and amplitude constraints. In addition, it enables the averaging of measurements across multiple periods, thereby enhancing the signal-to-noise ratio [9]. This averaging facilitates precise online measurements, particularly when dealing with small injection amplitudes, which can be a crucial necessity in sensitive systems. The traditional method involves introducing an initial disturbance in the D channel to obtain the impedances

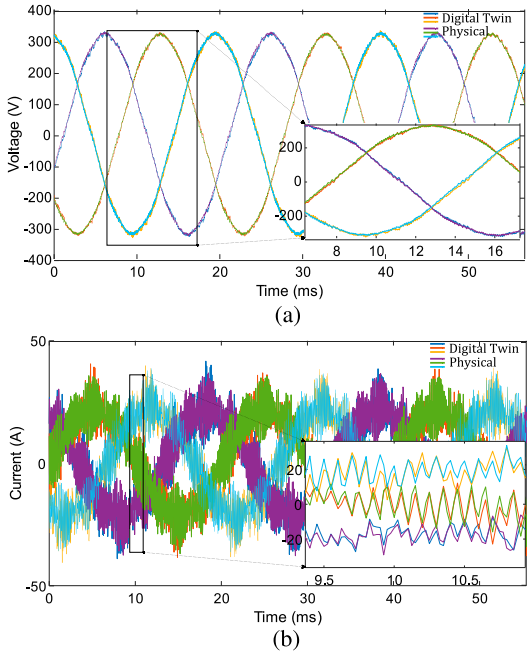

Fig. 6. Comparison between DT signals and real measurements: (a) v_{xo} voltages and (b) i_{21} currents.

related to this channel. This is followed by a subsequent disturbance in the Q channel to obtain the impedances related to the latter.

B. IRS Orthogonal Perturbation

The most recent advancements in broadband perturbation-based identification involve the integration of orthogonal sequences. The orthogonal periodic binary sequence, known as the IRS, is used acknowledging the MIMO nature of the system. This approach is based on Hadamard modulation applied to the prior MLBS perturbation designed, as outlined in [27]. It must be noted that the sequence length of the orthogonal sequence is doubled compared with the length of the MLBS sequence. Fig. 7 illustrates an instance of two orthogonal binary sequences generated using the described method. The length of the MLBS is 11 bits, and it is generated at a frequency of 2.5 kHz. Notably, the energy of each harmonic introduced in the MLBS sequence has a zero value in the IRS disturbance. Consequently, they can be simultaneously introduced into the d and q channels of a given magnitude without compromising the identification of each component. It can be seen clearly that the IRS magnitude in Fig. 7 is scaled by 1.5 for illustrative purposes.

C. GFM and GFL Impedances Estimation

In Fig. 2, the setup illustrates the application of perturbations for conducting impedance identification. In the case of obtaining the impedance of the GFM converter, PRBS perturbations are introduced into the input i_{22} of the DT, recording the corresponding responses in the voltage of the capacitors of the output filter (u_c). The disturbance signals are introduced

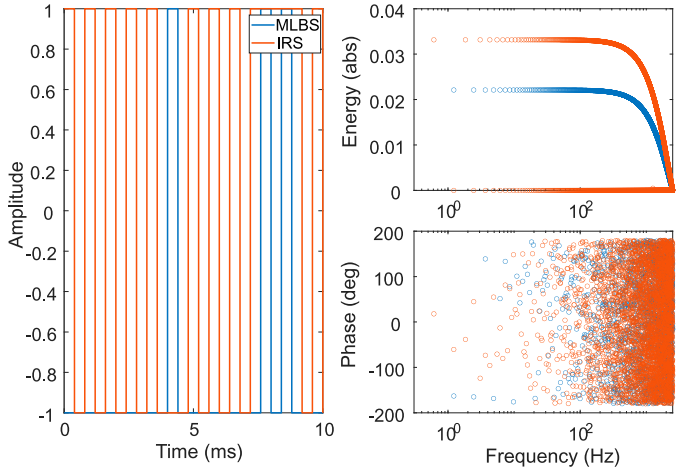

Fig. 7. Perturbation sequences in time and frequency domain.

into the current inputs of the digital model to assess its impact on the capacitor voltage, accounting for the dynamics of the control loops within the virtual domain. In the case of obtaining the impedance of the GFL converter, perturbations are introduced on the voltage modulating signals (u_{2dq}) of the GFM system, again recording the i_{22} and u_c measured in the actual setup. In this article, binary disturbances were applied directly to the modulation signals to mitigate any influence from the transfer function that connects the output current to the current references (i_{21dq}/i_{21dq}^{ref}). However, it is important to highlight that these perturbations undergo shaping by a digital filter to remove high-frequency components from the signal, thus preventing aliasing concerns during response sampling.

These perturbations are injected in parallel in both real and virtual space. So, assuming that the impedance does not change during the identification process (operating conditions do not change), thus, two sets of equations can be written, where subscript 1 and 2 denote the first and the second injection, respectively

$$\begin{aligned} V_{d1} &= Z_{dd}I_{d1} + Z_{dq}I_{q1} \\ V_{q1} &= Z_{qd}I_{d1} + Z_{qq}I_{q1} \end{aligned} \tag{7}$$

$$\begin{aligned} V_{d2} &= Z_{dd}I_{d2} + Z_{dq}I_{q2} \\ V_{q2} &= Z_{qd}I_{d2} + Z_{qq}I_{q2}. \end{aligned} \tag{8}$$

The resolution of the system of equations presented by (7) and (8) in matrix format can be easily determined

$$\begin{bmatrix} Z_{dd} & Z_{dq} \\ Z_{qd} & Z_{qq} \end{bmatrix} = \begin{bmatrix} V_{d1} & V_{d2} \\ V_{q1} & V_{q2} \end{bmatrix} \begin{bmatrix} I_{d1} & I_{d2} \\ I_{q1} & I_{q2} \end{bmatrix}^{-1}. \tag{9}$$

It is noteworthy that the orthogonal sequences inherently possess distinct frequency vectors. Therefore, a proposed interpolation process is applied to the signals perturbed by the IRS. Notably, the interpolation is not directly performed on the DFT of voltages and currents due to the pseudorandom phase characteristic of the frequencies excited by the IRS sequence, as depicted in Fig. 7. To address this challenge, (9) can be

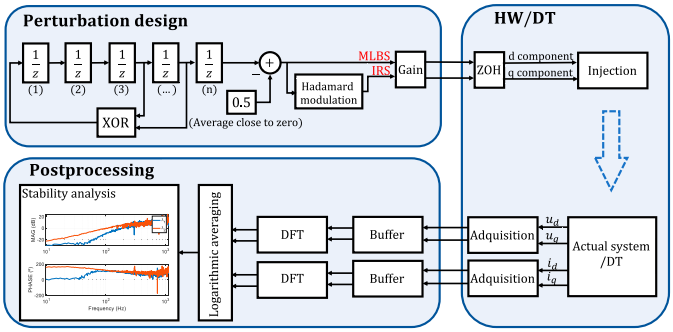

Fig. 8. Overview of the stability assessment process in the edge-computing platform.

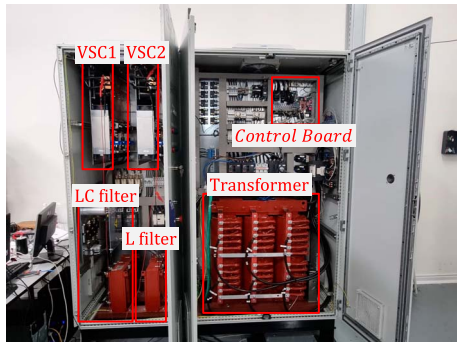

Fig. 9. Test-bed system for experimental verification of the real-time stability assessment.

expanded in a manner that represents the 2 x 2 *dq* impedance matrix through terms associated with voltages and currents

$$\begin{bmatrix} Z_{dd} & Z_{dq} \\ Z_{qd} & Z_{qq} \end{bmatrix} = \begin{bmatrix} \frac{\left(\frac{I_{q2}}{V_{d2}}\right)-\left(\frac{I_{q1}}{V_{d1}}\right)}{\alpha} & \frac{\left(\frac{I_{d1}}{V_{d1}}\right)-\left(\frac{I_{d2}}{V_{d2}}\right)}{\alpha} \\ \frac{\left(\frac{I_{q2}}{V_{q2}}\right)-\left(\frac{I_{q1}}{V_{q1}}\right)}{\beta} & \frac{\left(\frac{I_{d1}}{V_{q1}}\right)-\left(\frac{I_{d2}}{V_{q2}}\right)}{\beta} \end{bmatrix} \tag{10a}$$

$$\alpha = \left(\frac{I_{d1}}{V_{d1}}\right)\left(\frac{I_{q2}}{V_{d2}}\right) - \left(\frac{I_{q1}}{V_{d1}}\right)\left(\frac{I_{d2}}{V_{d2}}\right) \tag{10b}$$

$$\beta = \left(\frac{I_{d1}}{V_{q1}}\right)\left(\frac{I_{q2}}{V_{q2}}\right) - \left(\frac{I_{q1}}{V_{q1}}\right)\left(\frac{I_{d2}}{V_{q2}}\right). \tag{10c}$$

Therefore, a straightforward arithmetic mean is applied to the admittances with subscripts 2 in (10a)

$$\left(\frac{I_{x2}}{V_{x2}}\right)_k^{\text{interpolated}} = \frac{\left(\frac{I_{x2}}{V_{x2}}\right)_k + \left(\frac{I_{x2}}{V_{x2}}\right)_{k+1}}{2} \tag{11}$$

where the subscript x can mean either the d or q component in the *dq* domain. After aligning all the quantities with a common frequency vector, it becomes feasible to derive the 2 x 2 impedance matrix in the *dq* domain.

After obtaining the output impedances of the GFM and GFL converters, a real-time stability analysis, using the Nyquist criterion, is performed on the same edge-computing platform. Fig. 8 provides an overview of the entire disturbance injection process and the subsequent stability analysis from the concepts described in Section II.

V. Experimental Results

The proposed stability analysis with a DT approach is experimentally evaluated in the setup shown in Fig. 9. The most intuitive way of making the system unstable is to increase the VSC2 output impedance, which can be accomplished by decreasing the bandwidth of its output voltage control loop. The aforementioned exemplifies a method to induce oscillations in the system, although there may be other ways to analyze its stability and robustness. It is worth noting that the purpose of adjusting the bandwidth of the GFM converter is to observe the variation in the impedance obtained through the DT. Additionally, it would be feasible to adjust the control parameters of the GFL and observe their impact on the overall real-time stability assessment.

TABLE I
VSC2 Control Parameters Summary

Cases	Voltage Loop	Description
Case 1	$0.275 + 231.60/s$	High bandwidth
Case 2	$0.172 + 93.64/s$	Medium bandwidth
Case 3	$0.145 + 67.01/s$	Low bandwidth

In this work accordingly, the VSC1 control parameters were kept constant, and only the VSC2 voltage controller is adjusted to create stable and unstable conditions. It is defined three different cases, whose description is summarized in Table I.

Furthermore, the impact of the PLL on inverters connected to a grid, particularly to the grid generated by the GFM converter, will be examined, as they introduce stability issues, especially when operating with weak grids. Specifically, working with different bandwidths in the GFM enables us to model, to some extent, operation with either a stronger or weaker grid.

Finally, the technical issues that must be considered in the implementation of the method and its experimental validation include the following.

1) DT implementation details;
2) PRBS perturbation design;
3) System executability; and
4) Real-Time stability assessment.

A. DT Implementation Details

The integration of the DT into the edge-computing platform is facilitated by Tustin's discretization of the modeling stage. The virtual replica operates with a time step of 2.5 μs, using an IP embedded in the PL (Fig. 10) to ensure periodic triggering of the digital mirror.

First, it includes configuration registers that can be accessed to set the digital mirror execution period. Second, a prescaler is provided to synchronize the period and consistently trigger interrupts. And final, the local interrupt management (LIM) subsystem is used to oversee DT interrupts and facilitate their direct transmission to the PS.

However, there are technical hurdles specific to the platform that require attention. The execution of the DT occurs on CPU1 (as illustrated in Fig. 5) alongside the implementation

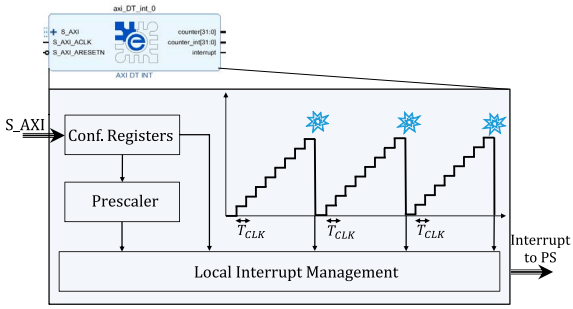

Fig. 10. Dedicated IP for DT interrupts management.

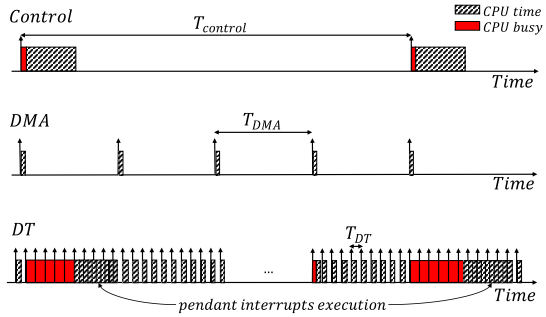

Fig. 11. Behavior of interrupts in the system.

of control algorithms for the physical system. Additionally, the platform operates in a non-preemptive manner. Given the presence of multiple interrupts, this feature represents a significant technical challenge.

In this experimental validation, the platform encounters three primary interrupt sources with different periods and priorities. Specifically, the control interrupt occurs every 100 μs, the DMA at 25 μs, and the DT interruption at an average periodicity of 2.5 μs. In terms of priorities, the highest priority is the DMA interrupt, followed by the control one. The DT interrupt has the lowest priority to minimize interference with the base control of physical system. Considering the above factors and the non-preemptive nature of the system, the loss of some DT steps is inevitable due to its higher frequency of interruption. Nonetheless, the LIM subsystem effectively manages this scenario by storing pending steps while other interrupt service calls are in progress. This behavior is more clearly illustrated in Fig. 11.

Moreover, it is also important to note that the inputs from external sensors in the physical system are sampled along with the outputs of the digital replica at intervals of 100 μs. This sampling frequency is deliberately chosen to harmonize with the control requirements of the real GFM and to ensure consistent impedance identification between the DT and the physical system.

B. PRBS Perturbation Design

Two orthogonal binary sequences were designed and implemented concurrently in both the actual system and in the DT. The MLBS was employed to measure the d-current/voltage component, including the cross-coupling component from d to q. Simultaneously, the IRS was utilized to measure the intended q-current/voltage component, along with the cross-coupling component from q to d.

The MLBS is synthesized through an 11-bit-length shift register, spanned a length of 2047 bits, providing a frequency resolution of approximately 1.2 Hz. The values were selected to ensure there is enough spectral resolution for online stability analysis and a short enough injection period to perform real-time DFT transformation on the edge-computing platform. Notably, the IRS length was defined as twice that of the MLBS. In each iteration, both the MLBS and IRS were concurrently introduced into the system at a frequency of 2.5 kHz (fgen). It is noteworthy to mention that fgen represents the frequency of the generated sequence. Careful adjustments were made to the injection amplitudes to ensure that output voltages and currents remained within 5% of their nominal values. It should be noted that the practical measurement bandwidth is approximately 0.45 fgen, to ensure that the injected harmonics have sufficient energy for accurate impedance estimation. The logarithmic averaging is applied through 50 periods of injection, which means that it takes about 41 s to obtain a final impedance identification. These values are adjustable and depend on the desired balance between time and accuracy for the specific application. Finally, a postprocessing stage is performed by a three-samples median filter to remove spikes in the impedances identified.

C. System Executability

Data recording takes place within the core where converter control is executed. At regular intervals, precisely every 100 μs, aligning with the control period of the physical converter, the dq voltage/current signals are transmitted to the Linux-based core. This transmission enables DFT implementation across an entire period of PRBS sequences. To ensure the feasibility of the edge-computing platform, it is crucial for DFT calculations to conclude within a timeframe shorter than the duration of a PRBS period. The condition that must be met to ensure that the impedance identification system is executable is as follows:

$$T_{\text{FFT}} \leq 2T_{\text{MLBS}} + T_{\text{delay}}. \tag{12}$$

where T_{FFT} denotes the total time spent performing the DFT of both perturbation sequences (MLBS and IRS). T_{MLBS} represents the period imposed by the perturbation design, considering that this value is doubled due to the IRS perturbation signal's duration, as previously detailed. Additionally, T_{delay} denotes the delay timing of the internal communication channel between cores, which must be limited to a maximum of 100 μs, aligning with the control period.

D. Real-Time Stability Assessment

Fig. 12 illustrates the outcomes of impedance identification for both the GFM and GFL converters from the experimental test-bed shown in Fig. 9. Furthermore, the theoretical impedances of both systems have been incorporated using an averaged theoretical model. This ensures that the identification of both impedances enables a comprehensive examination of

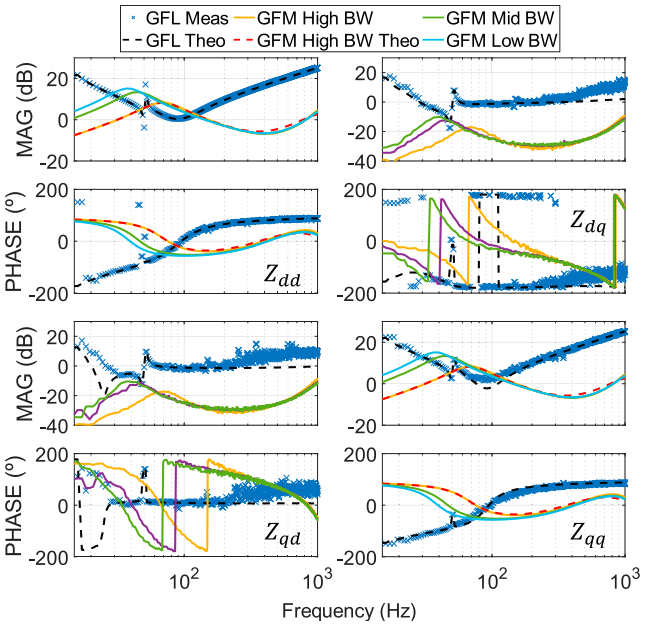

Fig. 12. Source-load impedance identification.

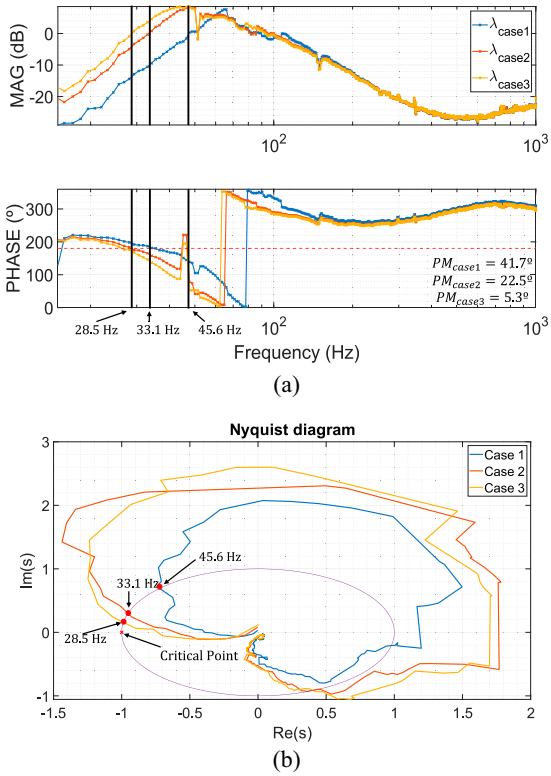

Fig. 13. Experimental results of the real-time stability assessment: (a) Eigenvalues of the minor loop of source/load impedance. (b) equivalent Nyquist diagram.

the interconnection's robustness. The noise level during the GFL impedance identification process is noticeable, as is the frequency shift of the GFM impedance in relation to the implemented bandwidth.

The main reason for the increased noise in impedance measurement with GFL is the relatively small magnitude of disturbances, which are aimed at minimizing disruption to the operational system. In contrast, within the virtual environment of the DT, disturbances can be amplified as needed, but control loops must avoid saturation to allow for small-signal analysis of the system.

Moreover, the influence of the PLL on the identified GFL impedance is manifested by the phase approximation nearing $-180°$ at low frequencies, resulting in a reduction in the stability margin of the connection, particularly pronounced when the bandwidth of the GFM is lower. This effect becomes more prominent when operating with nonstiff grids.

The eigenvalues of the MIMO system have been obtained using expression (2), and their frequency response in magnitude and phase has been depicted in Fig. 13. It is noteworthy that, being a 2 x 2 system, each case consists of two eigenvalues; however, in analyzing the stability of the system, one eigenvalue is consistently more restrictive. Consequently, only one eigenvalue is presented for each case investigated in this article.

The impact of reducing the bandwidth of the GFM converter is evidenced by the shift of the cutoff frequency of the module with 0 dB toward lower frequencies. Consequently, the system's stability diminishes gradually, reaching a PM of 5.3° in the case 3. This reduction in robustness is effectively demonstrated through a time domain analysis.

Fig. 14 shows the time response to a 50 V step change in the dc bus voltage reference of VSC1, along with the frequency analysis of the transient. As the bandwidth of VSC2 decreases, the system exhibits a prolonged duration to dampen the oscillation of the transient, aligned with the eigenvalue cutoff with 0 dB magnitude (or equivalently, the cutoff with the unit circle represented in a Nyquist plot). As a result, the system gradually approaches its stability limit. The oscillation frequency obtained in the stability analysis closely aligns, with an error below 1 Hz, with what is observed in the time domain. This alignment underscores the feasibility and efficacy of the system within a low-cost edge computing environment. Moreover, it is noteworthy to highlight that the applicability range of this methodology as a stability margin monitoring tool depends entirely on the design described in Section V-B. Various limits are established based on parameters such as the generation frequency, number of bits, disturbance amplitude, and the sampling and computational capabilities of the edge-computing platform. In this specific application, an operational range spanning from 10 to 1000 Hz has been determined, ensuring precise impedance identification. However, these limitations can be either extended or narrowed in other scenarios, depending on the frequency range of interest.

Kindly note that this method is applicable exclusively when the connection of the systems is stable. This approach serves to analyze whether corrective actions are required to enhance overall robustness. This article does not cover the assessment of dynamic stability in relation to equipment perturbations, such

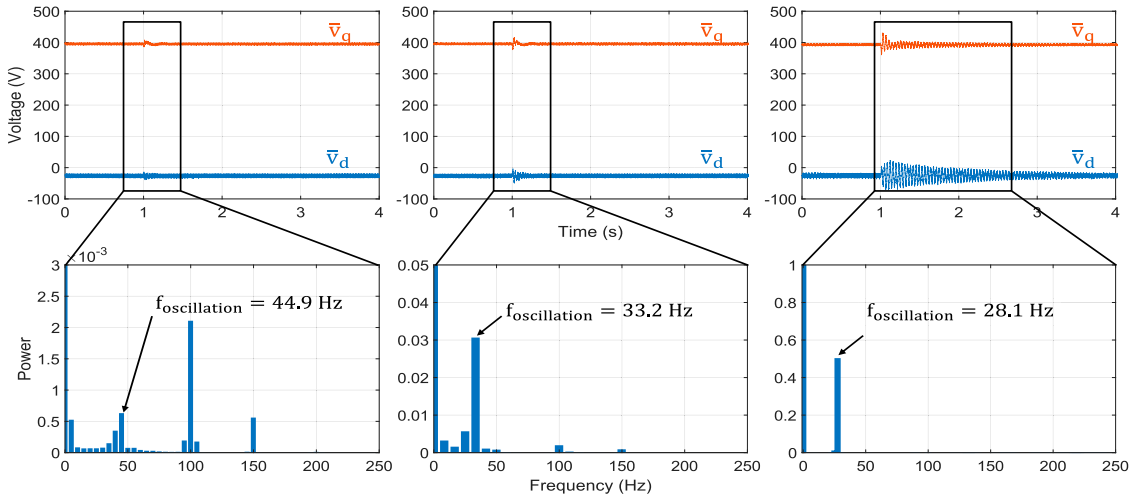

Fig. 14. Time domain response and frequency analysis of interface voltage in *dq* frame.

as voltage dips or overvoltages. To use the DT as a tool for handling such scenarios, it would be necessary to establish various conditions to train the DT model. This would enable the detection of potential instability issues and prompt action in response, requiring strict constraint handling. Furthermore, the DT could be used to analyze the dynamic stability of converters by simulating different operating conditions and perturbations. By modeling the converter's behavior in various scenarios, the DT can offer insights into its dynamic response and aid in identifying potential instability issues.

In addition, Fig. 15 shows oscilloscope captures corresponding to case 3 when there is a step in the dc bus reference of VSC1 and the unstable case with a lower bandwidth, where the system gradually becomes unstable as a consequence of the interaction between impedances of both converters. In the instantaneous voltage waveforms, it is challenging to distinguish oscillations caused by the higher energy in the 50 Hz component. Thus, a FFT of several periods following the step in the dc bus reference is incorporated to address this issue. The FFT reveals mirror frequencies at 23 and 76.7 Hz, corresponding to a minor deviation from (50 − 28.1) Hz to (50 + 28.1) Hz, respectively, in relation to the 28 Hz oscillation observed in the dq voltage signals.

Upon detecting the existing robustness margin at the specific operational point, appropriate actions are initiated. This entails initially enhancing the bandwidth of the voltage control in the GFM system by adjusting the constants within the virtual control of the DT. Following a comprehensive reassessment of stability through the injection of PRBS disturbances, the adjustments are then made to the control system in the physical setup. This demonstrates the complete bidirectional interaction between the digital replica and its physical counterpart. Certainly, expanding the bandwidth of the voltage loop represents one plausible implementation of adaptive control utilizing the DT. It allows for potential modifications to the control structure, the incorporation of feedforwards terms, or the integration of any actions aimed at enhancing the stability margin of the integrated system.

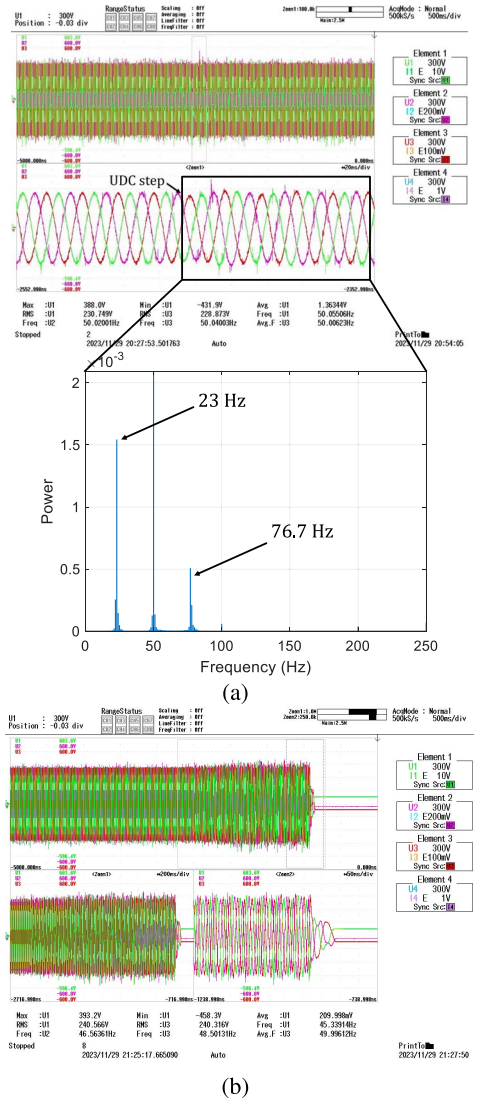

Fig. 15. Comparison of time domain measurements: (a) Three-phase voltages for case 3. (b) Three-phase voltages for an unstable scenario.

VI. Conclusion

Interconnected inverters are pivotal for the functioning of power electronics-based systems. The interactions among multiple subsystems and the power grid give rise to various stability challenges. Extracting information from these systems often requires frequency-response measurements, especially when the internal dynamics of certain subsystems remain unknown. Consequently, there is a high demand for online measurement methods that can furnish real-time data about the system's status. This article introduced a practical real-time approach, leveraging DT technology, for conducting a comprehensive stability analysis of a GFM and GFL system. First, it has been demonstrated that the DT can achieve similar output waveforms and almost identical behavior to its physical counterpart. Second, the proposed method involved injecting orthogonal PRBS perturbations into both the actual converter and its virtual replica to extract source/load impedance. Implemented on an edge-computing platform and experimentally validated on a hybrid-dual converter, this method yielded an accurate robustness metric. This robustness metric serves, for instance, as a tool for online adaptive control, allowing adjustments based on the specific conditions and load impedance to which the system is connected, whereas in the vast majority of applications, adaptive control is based on prior knowledge of the system to which you are going to connect, performing gain scheduling approaches.

References

[1] S. K. Dube, R. Nair, and P. Das, "Analysis and design of an integrated bidirectional three phase AC–DC resonant converter," *IEEE Trans. Ind. Electron.*, vol. 70, no. 5, pp. 4369–4379, May 2023, doi: 10.1109/TIE.2022.3183274.

[2] W. Lambrichts and M. Paolone, "Linear recursive state estimation of hybrid and unbalanced AC/DC micro-grids using synchronized measurements," *IEEE Trans. Smart Grid*, vol. 14, no. 1, pp. 54–67, Jan. 2023, doi: 10.1109/TSG.2022.3190996.

[3] Q. An, C. Dong, J. Li, and F. Jiang, "A secure and efficient renewable energy sharing framework for distributed prosumers," in *Proc. IEEE IAS Global Conf. Renewable Energy Hydrogen Technol. (GlobConHT)*, 2023, pp. 1–5, doi: 10.1109/GlobConHT56829.2023.10087386.

[4] S. Prakash, O. A. Zaabi, R. K. Behera, K. A. Jaafari, K. A. Hosani, and U. R. Muduli, "Modeling and dynamic stability analysis of the grid-following inverter integrated with photovoltaics," *IEEE J. Emerg. Sel. Topics Power Electron.*, vol. 11, no. 4, pp. 3788–3802, Aug. 2023, doi: 10.1109/JESTPE.2023.3272822.

[5] F. C. Lee and Y. Yu, "Input-filter design for switching regulators," *IEEE Trans. Aerosp. Electron. Syst.*, vol. AES-15, no. 5, pp. 627–634, Sep. 1979, doi: 10.1109/TAES.1979.308851.

[6] S. Cobreces, F. Huerta, D. Pizarro, F. J. Rodrguez, and E. J. Bueno, "Three-phase power system parametric identification based on complex-space recursive least squares," in *Proc. IEEE Int. Symp. Intell. Signal Process.*, 2007, pp. 1–6, doi: 10.1109/WISP.2007.4447570.

[7] A. Riccobono, M. Mirz, and A. Monti, "Noninvasive online parametric identification of three-phase AC power impedances to assess the stability of grid-tied power electronic inverters in LV networks," *IEEE J. Emerg. Sel. Topics Power Electron.*, vol. 6, no. 2, pp. 629–647, Jun. 2018, doi: 10.1109/JESTPE.2017.2783042.

[8] H. Alenius, M. Berg, R. Luhtala, and T. Roinila, "Stability and performance analysis of grid-connected inverter based on online measurements of current controller loop," in *Proc. 45th Annu. Conf. IEEE Ind. Electron. Soc. (IECON)*, vol. 1, 2019, pp. 2013–, doi: 10.1109/IECON.2019.8926676.

[9] R. Luhtala, H. Alenius, T. Messo, and T. Roinila, "Online frequency response measurements of grid-connected systems in presence of grid harmonics and unbalance," *IEEE Trans. Power Electron.* vol. 35, no. 4, pp. 3343–3347, Apr. 2020, doi: 10.1109/TPEL.2019.2943711.

[10] B. Wen, D. Boroyevich, R. Burgos, P. Mattavelli, and Z. Shen, "Analysis of D-Q small-signal impedance of grid-tied inverters," *IEEE Trans. Power Electron.*, vol. 31, no. 1, pp. 675–687, Jan. 2016, doi: 10.1109/TPEL.2015.2398192.

[11] H. Zhang, M. Saeedifard, X. Wang, F. Wei, and X. Wang, "A sequential SISO stability analysis model for grid-connected converters by considering the impact of power flow direction," *IEEE Trans. Power Electron.*, vol. 39, no. 3, pp. 3702–3711, Mar. 2024, doi: 10.1109/TPEL.2023.3343353.

[12] Q. Peng, G. Buticchi, N. M. L. Tan, S. Guenter, J. Yang, and P. Wheeler, "Modeling techniques and stability analysis tools for grid-connected converters," *IEEE Open J. Power Electron.*, vol. 3, pp. 450–467, 2022, doi: 10.1109/OJPEL.2022.3190103.

[13] R. Luhtala, T. Roinila, and T. Messo, "Implementation of real-time impedance-based stability assessment of grid-connected systems using MIMO-identification techniques," *IEEE Trans. Industry Appl.*, vol. 54, no. 5, pp. 5054–5063, Sep./Oct. 2018, doi: 10.1109/TIA.2018.2826998.

[14] E. Glaessgen and D. Stargel, "The digital twin paradigm for future NASA and US air force vehicles," in *Proc. 53rd AIAA/ASME/ASCE/AHS/ASC Structures, Structural Dyn. Mater. Conf.*, 2012, doi: 10.2514/6.2012-1818.

[15] M. Grieves, "Intelligent digital twins and the development and management of complex systems [version 1; peer review: 4 approved]," *Digital Twin*, vol. 2, no. 8, 2022.

[16] J. Huang, L. Zhao, F. Wei, and B. Cao, "The application of digital twin on power industry," in *Proc. IOP Conf. Ser. Earth Environ. Sci.*, vol. 647, 2021, Art. no. 012015, doi: 10.1088/1755-1315/647/1/012015.

[17] M. Milton, C. D. L. O, H. L. Ginn, and A. Benigni, "Controller-embeddable probabilistic real-time digital twins for power electronic converter diagnostics," *IEEE Trans. Power Electron.*, vol. 35, no. 9, pp. 9850–9864, 2020, doi: 10.1109/TPEL.2020.2971775.

[18] G. Di Nezio, M. Di Benedetto, A. Lidozzi, and L. Solero, "Digital twin based real-time analysis of DC-DC boost converters," in *Proc. IEEE Energy Convers. Congr. Expo. (ECCE)*, 2022, pp. 1–7, doi: 10.1109/ECCE50734.2022.9947394.

[19] S. de Lopez Diz, R. M. Lopez, F. J. R. Sanchez, E. D. Llerena, and E. J. B. Pena, "A real-time digital twin approach on three-phase power converters applied to condition monitoring," *Appl. Energy*, vol. 334, 2023, Art. no. 120606, doi: 10.1016/j.apenergy.2022.120606. [Online]. Available: https://www.sciencedirect.com/science/article/pii/S0306261922018633

[20] M. Berg and T. Roinila, "Nonlinear effect of dead time in small-signal modeling of power-electronic system under low-load conditions," *IEEE J. Emerg. Sel. Topics Power Electron.*, vol. 8, no. 4, pp. 3204–3213, Dec. 2020, doi: 10.1109/JESTPE.2020.2967341.

[21] M. Petkovic and D. Dujic, "Benchmark study on impedance identification methods for grid connected converters," in *Proc. Int. Exhib. Conf. Power Electronics, Intell. Motion, Renewable Energy Energy Manage. (PCIM)*, 2019, pp. 1–7.

[22] T. Roinila, H. Abdollahi, and E. Santi, "Frequency-domain identification based on pseudorandom sequences in analysis and control of DC power distribution systems: A review," *IEEE Trans. Power Electron.*, vol. 36, no. 4, pp. 3744–3756, Apr. 2021, doi: 10.1109/TPEL.2020.3024624.

[23] R. D. Middlebrook, "Input filter considerations in design and application of switching regulators." Semantic Scholar. [Online]. Available: https://api.semanticscholar.org/CorpusID:60811006

[24] T. Messo, J. Jokipii, A. Aapro, and T. Suntio, "Time and frequency-domain evidence on power quality issues caused by grid-connected three-phase photovoltaic inverters," in *Proc. 16th Eur. Conf. Power Electron. Appl.*, 2014, pp. 1–9, doi: 10.1109/EPE.2014.6910808.

[25] J. Allmeling, N. Felderer, and M. Luo, "High fidelity real-time simulation of multi-level converters," in *Proc. Int. Power Electron. Conf. (IPEC-Niigata 2018 -ECCE Asia)*, 2018, pp. 2199–2203, doi: 10.23919/IPEC.2018.8508021.

[26] P. Zhong, J. Sun, L. Qu, P. Yu, and X. Zha, "An improved PRBS-injection-based grid impedance measurement method considering non-ideal grid conditions," *IEEE Trans. Ind. Electron.*, vol. 70, no. 6, pp. 6452–6456, Jun. 2023, doi: 10.1109/TIE.2022.3196379.

[27] T. Roinila, H. Abdollahi, S. Arrua, and E. Santi, "Real-time stability analysis and control of multiconverter systems by using MIMO-identification techniques," *IEEE Trans. Power Electron.*, vol. 34, no. 4, pp. 3948–3957, Apr. 2019, doi: 10.1109/TPEL.2018.2856532.

Sergio de Lopez Diz was born in Alcala de Henares, Spain, in 1997. He received the B.Sc. degree in electronics communications engineering and the M.Sc. degree in telecommunications from the University of Alcala, Alcala de Henares, Spain, in 2019 and 2021, respectively, where he is working toward the Ph.D. degree with the Department of Electronics within the Electronics Engineering Applied to Renewable Energies Research Group (GEISER).

His primary areas of interest encompass power electronics, power control design, and the implementation of digitalization in power converters.

Roberto Martin Lopez was born in Alcala de Henares, Spain, in 1997. He received the B.Sc. degree in electronics communications engineering and the M.Sc. degree in telecommunications from the University of Alcala, Alcala de Henares, Spain, in 2019 and 2021, respectively, where he is currently working toward the Ph.D. degree with the Department of Electronics in Electronics Engineering Applied to the Renewable Energies Research Group (GEISER).

His main interest areas are power electronics, power control design, and SoC design applied to power electronics.

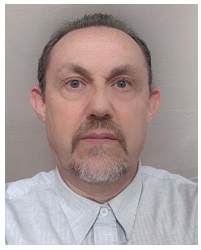

Francisco Javier Rodriguez Sanchez (Member, IEEE) received the B.Sc. degree in technical telecommunication engineering from the University of Alcala, Alcala de Henares, Spain, in 1985, the M.Sc. degree in telecommunication from the Technical University of Madrid, Madrid, Spain, in 1990, and the Ph.D. degree in electronics engineering from the University of Alcala, in 1997.

Since 1986, he has been a Lecturer with the Department of Electronics, University of Alcala, where he is currently a Professor. He is the author of more than 160 refereed publications in international journals, book chapters, and conference proceedings.

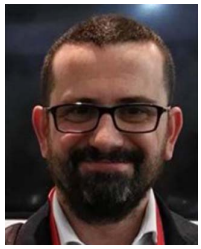

Emilio Jose Bueno Peña (Senior Member, IEEE) was born in Madrid, Spain, in 1972. He received the Ph.D. degree in electronics engineering from the University of Alcala, Alcala de Henares, Spain, in 2005.

Since 2019, he has been a Full Professor with the Department of Electronics, University of Alcala, and a Co-Supervisor of the Electronics Engineering Applied to the Renewable Energies Research Group. From 2010 to 2013, he was a Vice-Dean of the Polytechnic School, University of Alcala, in charge of electrical engineering studies. His research interests include linear control of grid converters and drives, power quality, distributed generation systems, and medium-voltage converter topologies.